The Influence of Amyloid-Beta on Calcium Dynamics in Alzheimer's Disease: A Spatio-Temporal Study

Swadesh Pal[1], Hina Shaheen[1(✉)], and Roderick Melnik[1,2]

[1] M3AI Laboratory, MS2Discovery Interdisciplinary Research Institute, Wilfrid Laurier University, Waterloo, ON N2L 3C5, Canada
shah8322@mylaurier.ca,
rmelnik@wlu.ca
[2] BCAM - Basque Center for Applied Mathematics, 48009 Bilbao, Spain
http://m3ai.wlu.ca

Abstract. One of the keys to understanding and treating Alzheimer's disease (AD) and dementia is believed to be calcium (Ca^{2+}) in the cytoplasm. Researchers have discovered how an imbalance of Ca^{2+}ions in the cytoplasm can lead to cell death and, more particularly, neurodegeneration in brain cells in Alzheimer's and dementia patients. Many substances are present in brain cells, but Ca^{2+} is the most tractable and is employed for experimental validations. In this study, we employ a spatio-temporal computational model to investigate AD development using Ca^{2+} dynamics in the cytoplasm. We study the spatio-temporal dynamics of biochemical processes via a new coupled model and analyze the sensitivity of this model to some of the critical parameters. As a result of this study, several important contributions have been made. Firstly, we have demonstrated that the SERCA pump flux parameter has a significant impact on the frequency of intracellular calcium concentrations. Furthermore, we studied Ca^{2+} dynamics with diffusion in the presence of different amyloid-beta levels. We found that how amyloid-beta affects various fluxes contributions through voltage-gated calcium channels, amyloid-beta-formed channels and ryanodine receptors. This work contributes to a better understanding of the spatio-temporal action of Ca^{2+} dysregulation in the cytoplasm, and through this, it can offer further insight into AD developments and progression.

Keywords: Alzheimer's disease · Ca^{2+} dysregulation · Cellular excitability · Neurons and astrocytes · Amyloid-beta · SERCA pump · Spatio-temporal coupled models

1 Introduction

Prion-like proliferation and aggregation of harmful proteins are linked to neurodegenerative diseases including Alzheimer's and Parkinson's disease [1].

O. Gervasi et al. (Eds.): ICCSA 2022 Workshops, LNCS 13377, pp. 308–322, 2022.
https://doi.org/10.1007/978-3-031-10536-4_21

Amyloid- beta (Aβ) oligomers linked with Alzheimer's disease (AD) might cause adverse intracellular calcium Ca^{2+} levels by affecting the intrinsic Ca^{2+} regulation system within cells. These disturbances can result in alterations in homeostasis levels and can have a negative impact on cell functions and survival. Although research has revealed that Aβ can interfere with diverse Ca^{2+} fluxes, the complexities of these interactions largely remain a mystery [2,3]. Due to the widespread involvement of Ca^{2+} disruption in AD development, it's likely that concentrating on Ca^{2+} dysregulation might assist in the development of a possible therapeutic strategy for preventing or treating AD, despite the fact that existing hypotheses about AD have yet to offer curative medicines [4].

Meanwhile, the term "cellular excitability" has been recently introduced to characterise variations in cytosolic Ca^{2+} concentration in response to chemical or mechanical stimulations in astrocytes [5]. Earlier, De Pittà et al. [6], for example, found that they encode synaptic information by modulating intracellular calcium dynamics in response to synaptic activity. This kind of Ca^{2+} homeostasis, whether in neurons or astrocytes, may be disturbed by Aβ, particularly by its soluble oligomeric form, which is more damaging [7]. Aβ has been shown to disrupt several calcium fluxes in astrocytes. Deposition of Aβ oligomers not only creates holes in the lipid bilayer that are permeable to cationic ions, but also activates L-type CaV, increasing intracellular Ca^{2+} concentration [4]. Furthermore, exposure to Aβ increases the expression of astroglial mGluR5 [8]. Aβ can activate ryanodine receptors (RyRs) and inositol triphosphate receptors (IP3Rs) in astrocytes, causing Ca^{2+} release from the endoplasmic reticulum (ER) [4].

Previously, we developed a mathematical model that replicates Alzheimer's Aβ accumulation based on Ca^{2+}-dependent exosome release from neurons and astrocytes [3]. The components for calcium-induced calcium release (CICR) and sarco-endoplasmic Ca^{2+} ATPase pump (SERCA) are used in the majority of the computational investigations presented in this paper. Our model design emphasizes a well-documented pathway for Aβ regulation of intracellular calcium movements, that is amyloid-induced Ca^{2+} permeability through endogenous cation channels such as L- and N-type voltage-gated calcium channels (VGCCs) in the presence of diffusion. Our aim in this paper is to construct a spatio-temporal multiscale mathematical model of brain and to examine computationally astrocytic intracellular Ca^{2+} patterns under the influence of Aβ. In analyzing different scenarios with this model, we consider the initial conditions in such a way that they mimic the injection effect in some parts of the spatial domain [9]. Through voltage-gated calcium channels, Aβ-formed channels, and ryanodine receptors, our model explains how Aβ influences diverse flux contributions. The increasing Ca^{2+} and frequency of calcium oscillations were significantly induced by Aβ, according to bifurcation analysis of Aβ levels, which reflected the corresponding disease progression.

It is not an easy task to develop the complete model of Aβ mediated by calcium dynamics in the brain. However, numerous studies are going on to understand the exact Aβ impacts on astrocytes for AD [4,10]. In this paper, we use Aβ regulation of intracellular calcium regulatory fluxes as it is advantageous

in analyzing a variety of cell types with spatial components. Several important contributions have been made as a result of our studies. One of them has been to propose a novel computational spatio-temporal network and corresponding simulations for better understanding the underlying complicated biochemical interactions between Aβ and Ca^{2+}. Our extensive simulations have revealed that the model's excitability in spatio-temporal domain interact to produce calcium signals. Another important feature of our studies has been that the model reproduces the most common calcium signals and shows that their frequency is highly dependent on spontaneously active thalamic astrocytes spatial arrangement. We have also showed that depending on the spatial structure of calcium channels, parallel processes expressing the same calcium channels can exhibit various forms of calcium signals. In some areas of the spatial domain, we have considered the initial conditions in such a way that they approximate the injection effect. It is important to note that since the most terms included in the model change due to their dependency on the cytosolic Ca^{2+} concentrations (details are given in Sect. 3), a series of computational challenges have had to be overcome. Regardless of these challenges, our modeling approach that targets numerous pathways at the same time has shown to be successful to have a better understanding of Aβ impact. It is noteworthy that computational modelling is a strong tool that allows researchers to explore complicated systems because it is crucial to isolate each component for separate investigations experimentally. The effect of amyloid-beta on different pathways can change the calcium flux in the cytoplasm and ER. Therefore, studying the variations of the parameters is important in practical examples too because these parameters can capture such pathways, and their combinations help us to control the disease progression, as we demonstrate it in the next sections on the example of AD.

The remainder of this paper is organized as follows. In Sect. 2, we describe a spatio-temporal mathematical model for astrocytic Ca^{2+} mediated by Aβ in AD. In Sect. 3, we discuss results and present numerical simulations based on the developed model. Finally, we summarize results and outline future directions in Sect. 4.

2 Mathematical Model

In this section, we construct a spatio-temporal multiscale mathematical model that simulates Ca^{2+} patterns under the influence of Aβ. We devise our computational model based on the previous studies [3,4,9]. We begin by investigating how Aβ impacts each source of Ca^{2+} via several paths using this computational model. Intracellular Ca^{2+} levels are regulated by external Ca^{2+} influx and controlled release from intracellular Ca^{2+} stores like the ER. Ca^{2+} entrance into astrocytes is characterised by active transport via several kinds of VGCCs scattered across the membrane, as well as passive leakage. However, in astrocytes, IP_3-dependent CICR from the ER is thought to be the major mechanism governing intracellular Ca^{2+} dynamics [11]. CICR is primarily regulated by efflux from the ER to the cytoplasm, which is mediated by IP_3R and RyR, as well as

by the influx into the ER, which, in its turn, is mediated by SERCA pumps. The model is derived by following the flux in (J_{in}) and out (J_{out}) of the cytoplasm. The change in intracellular Ca^{2+} is then governed by:

$$\frac{\partial C_c}{\partial t} = \beta_c \left[(D^c_{Ca} + \gamma^c_m D^c_m + \gamma^c_e D^c_e)\nabla^2 C_c - 2\left(\frac{\gamma^c_m D^c_m}{K^c_m + C_c} + \frac{\gamma^c_e D^c_e}{K^c_e + C_c} \right) \nabla C_c \cdot \nabla C_c \right] + J_{VGCC} + J_{in} - J_{out} + J_{CICR} - J_{SERCA} + J_{RyR} + J_{leak}, \tag{1a}$$

$$\frac{\partial C_e}{\partial t} = \beta_e \left[(D^e_{Ca} + \gamma^e_m D^e_m)\nabla^2 C_e - 2\frac{\gamma^e_m D^e_m}{K^e_m + C_e} \nabla C_e \cdot \nabla C_e \right] + \frac{1}{c_1}(J_{SERCA} - J_{CICR} - J_{RyR} - J_{leak}), \tag{1b}$$

where C_c and C_e denote the concentration of Ca^{2+} in the cytoplasm and ER, respectively, and

$$\beta_c = \left(1 + \frac{B^c_s K^c_s}{(K^c_s + C_c)^2} + \frac{B^c_m K^c_m}{(K^c_m + C_c)^2} + \frac{B^c_e K^c_e}{(K^c_e + C_c)^2} \right)^{-1}, \ \gamma^c_l = \frac{B^c_l K^c_l}{(K^c_l + C_c)^2},$$

$$\beta_e = \left(1 + \frac{B^e_s K^e_s}{(K^e_s + C_e)^2} + \frac{B^e_m K^e_m}{(K^e_m + C_e)^2} \right)^{-1}, \ \gamma^e_m = \frac{B^e_m K^e_m}{(K^e_m + C_e)^2}$$

with $l = m$ and e. The term J_{VGCC} represents the Ca^{2+} influx through the four types of VGCCs, and it is given by

$$J_{VGCC} = \frac{-I_{VGCC}}{zFV_{ast}}, \tag{2}$$

where

$$I_{VGCC} = I_{Ca,T} + I_{Ca,L} + I_{Ca,N} + I_{Ca,R} \tag{3}$$

is the VGCC-conducted Ca^{2+} current, z is the valence of Ca^{2+}, F is the Faraday constant and V_{ast} is the volume of the astrocyte. $I_{Ca,l}$ ($l = T, L, N$ and R) denote the four types of channels. The term c_1 is the ratio of ER volume to the cytoplasmic volume.

The other terms contributed in the Eq. (1) are given as follows [3,4,12]:

$$J_{in} = \nu_5, \tag{4a}$$

$$J_{out} = k_1 C_c, \tag{4b}$$

$$J_{CICR} = \nu_1 m^3_\infty n^3_\infty h^3 (C_e - C_c), \tag{4c}$$

$$J_{SERCA} = \frac{\nu_3 C_c^2}{C_c^2 + k_3^2}, \tag{4d}$$

$$J_{RyR} = \left(k_0 + \frac{k_2 C_c^3}{k_d^3 + C_c^3} \right)(C_e - C_c), \tag{4e}$$

$$J_{leak} = \nu_2 (C_e - C_c), \tag{4f}$$

with the gating variable h that satisfies the Hodgkin-Huxley formalism as

$$\frac{dh}{dt} = a_2 d_2 \frac{C_i + d_1}{C_i + d_3}(1 - h) - a_2 C_c h. \tag{5}$$

The relevant parameters are given in Table 1 and $\bar{m}$, $\bar{h}$ are defined as follows [3]:

$$\frac{dy}{dt} = \frac{\bar{y} - y}{\tau_y}, \tag{6}$$

where $y = (m, h)$. As a result, we model V_m as follows:

$$V_m = \frac{RT}{z_K F} \ln \frac{[K_o^+]}{[K_i^+]} + \epsilon, \tag{7}$$

where R is the ideal gas constant, T is the absolute temperature, z_K is the valence of K^+, and F is the Faraday constant. $K_o = [K_o^+]$ and $[K_i^+]$ are the extracellular and intracellular K^+ concentrations, respectively. ϵ is a modulation factor [4].

IP_3 is the second messenger involved in signal transduction via G protein-coupled receptors. Phosphatidylinositol 4,5-bisphosphate is hydrolyzed by two phosphoinositide - specific phospholipase C (PLC) isoenzymes, $PLC\beta$ and $PLC\delta$ in astrocytes to generate IP_3 [4]. As a consequence, the concentration of IP_3 dynamic (C_i) is defined as

$$\frac{\partial C_i}{\partial t} = D_i \nabla^2 C_i + J_{PLC\beta} + J_{PLC\delta} - k_{deg} C_i, \tag{8}$$

where

$$J_{PLC\beta} = \nu_\beta \frac{g^{0.7}}{g^{0.7} + \left(k_R + k_P \frac{C_c}{C_c + k_\pi}\right)^{0.7}}, \; J_{PLC\delta} = \nu_4 \frac{C_c + (1 - \alpha k_4)}{C_c + k_4}.$$

Experimental results suggested that the Aβ peptide triggers the intracellular calcium oscillations [13]. Alves et al. demonstrated in [14] that the activated Aβ contributes to an additional current in the L-type channel. Taking this into account, $I_{Ca,L}$ can be written as

$$I_{Ca,L} = (g_L + A_\beta a) m_L h_L (V_m - V_{Ca}), \tag{9}$$

where A_β controls the strength of the effect of Aβ on the channel.

Therefore, the Aβ-formed channels supply an additional Ca^{2+} influx into the cytoplasm (see also [7]). It increases the channel open probability and also affects the IP_3 levels. Combining all these, we modify the influxes as follows:

$$J_{in} = \nu_5 + k_{in} a^k, \tag{10a}$$

$$J_{RyR} = \left(k_0 + \frac{k_2 C_c^3}{(k_d + k_{RyR} a)^3 + C_c^3}\right)(C_e - C_c), \tag{10b}$$

$$J_{PLC\beta} = (\nu_\beta + k_{PCL\beta} a) \frac{g^{0.7}}{g^{0.7} + \left(k_R + k_P \frac{C_c}{C_c + k_\pi}\right)^{0.7}}, \tag{10c}$$

$$J_{PLC\delta} = (\nu_4 + k_{PCL\delta} a) \frac{C_c + (1 - \alpha k_4)}{C_c + k_4}. \tag{10d}$$

Table 1. Details of the voltage-gated calcium channels [3].

Channel type	Equation of channel kinetics
$T-$type	$I_{Ca,T} = g_T \bar{m}_T (h_{Tf} + 0.04 h_{Ts})(V_m - V_{Ca})$
	$\bar{m}_T = 1/(1 + \exp(-(V_m + 63.5)/1.5))$
	$h_{Tf} = 1/(1 + \exp((V_m + 76.2)/3))$
	$h_{Ts} = 1/(1 + \exp((V_m + 76.2)/3))$
	$\tau_{h_{Tf}} = 50 * \exp(-((V_m + 72)/10)^2) + 10$
	$\tau_{h_{Ts}} = 400 * \exp(-((V_m + 100)/10)^2) + 400$
	$\tau_{m_T} = 65 * exp(-((V_m + 68)/6)^2) + 12$
$L-$type	$I_{Ca,L} = g_L \bar{m}_L h_L (V_m - V_{Ca})$
	$\bar{m}_L = 1/(1 + \exp(-(V_m + 50)/3))$
	$h_L = 0.00045/(0.00045 + C_c/1000)$
	$\tau_{m_L} = 18 * \exp(-((V_m + 45)/20)^2) + 1.5$
$N-$type	$I_{Ca,N} = g_N \bar{m}_N h_N (V_m - V_{Ca})$
	$\bar{m}_N = 1/(1 + \exp(-(V_m + 45)/7))$
	$h_N = 0.0001/(0.0001 + C_c/1000)$
	$\tau_{m_N} = 18 * \exp(-((V_m + 70)/25)^2) + 0.3$
$R-$type	$I_{Ca,R} = g_R \bar{m}_R h_R (V_m - V_{Ca})$
	$\bar{m}_R = 1/(1 + \exp(-(V_m + 10)/10))$
	$h_R = 1/(1 + \exp((V_m + 48)/5))$
	$\tau_{h_R} = 0.5 * \exp(-((V_m + 55.6)/18)^2) + 0.5$
	$\tau_{m_R} = 0.1 * \exp(-((V_m + 62)/13)^2) + 0.05$

This proposed spatio-temporal model has multiple Aβ-affected Ca^{2+} pathways. Simulations based on our mathematical model have proven to be an essential resource for investigating underlying complex biochemical interactions. This model portrays Ca^{2+} signals as discrete Ca^{2+} transport routes, rather than a macroscopic flow of Ca^{2+} that includes both intracellular release and external inflow.

The model has several computational challenges as maximum terms involved in the model are changing due to the dependence of such terms (e.g., β_c, γ_c, J_{RyR}, etc.) on the cytosolic Ca^{2+} concentration. Hence, the terms are not only time-dependent as it was the case in earlier developed models (e.g., [4]); they are space-dependent also. We have used all the parameter values from Table 2 and [8] unless specified otherwise in the figure caption or the text.

Table 2. Parameter values [4].

Parameter	Value	Parameter	Value	Parameter	Value
B_s^c	225 μM	B_m^e	250 μM	B_m^c	75 μM
B_e^c	0 μM	K_s^e	10 μM	K_s^c	1 mM
K_m^e	6 μM	K_m^c	6 μM	B_s^e	100 mM
K_e^c	0.16 μM	D_{Ca}^c	223.0	D_{Ca}^e	223.0
D_m^c	75.0	D_e^c	75.0	D_m^e	75.0
D_i	283.0	k_1	0.5 s^{-1}	ν_1	6 s^{-1}
d_1	0.13 μM	ν_3	2.2 $\mu M/s$	d_5	0.08234 μM
k_3	0.05 μM	k_0	0.013 s^{-1}	k_2	0.18 s^{-1}
k_d	0.13 μM	ν_2	0.11 s^{-1}	a_2	0.2 s^{-1}
d_2	1.049 μM	d_1	0.13 μM	d_3	0.9434 μM
ν_β	0.05 μM	g	1 μM	k_R	1.3 μM
k_P	10 μM	k_π	0.6 μM	ν_4	0.5 $\mu M/s$
α	0.8	k_4	1.1 μM	A_β	10
k_{in}	1	k_{RyR}	0.2	F	96485 $C/mole$
$k_{PCL\delta}$	0.5	$k_{PCL\beta}$	0.05	V_{ast}	3.49×10^{-13} L
z	2	g_T	0.06	g_L	3.5
g_N	0.39	g_R	0.2225	ν_5	0.36 $\mu M/s$

3 Computational Framework and Numerical Results

Liu et al. [4] has shown that, with an increase in the Aβ levels in the purely temporal model (based on ODEs only), a rapid increase is observed in the oscillation frequency of the intracellular Ca^{2+} concentrations and then C_c converges to its steady-state. At a low level of Aβ, the disease state is mild, but the disease becomes severe with higher Aβ. The dynamics of Aβ is studied here with model (1)–(9).

In this section, we find the numerical solution to the complete model (1)–(9). No-flux boundary conditions and a particular type of initial conditions have been used for the simulations. With the introduction of Ca^{2+} or IP_3 in the cytoplasm, calcium waves were experimentally verified in earlier works (e.g., [15]). Typically, Ca^{2+} or IP_3 are introduced by injecting them in the living cells. We consider the initial conditions in such a way that they mimic the injection effect in some parts of the spatial domain. A pulse-like initial condition in the specified domain can capture such a phenomenon. With the help of pulse structure, we consider

the initial conditions as follows [9]:

$$C_c(x,0) = \begin{cases} 0.2\ \mu M & 0 \le x \le L_c \\ 0.1\ \mu M & L_c < x \le 500 \end{cases}, \; C_e(x,0) = \begin{cases} 0.2\ \mu M & 0 \le x \le L_e \\ 1.5\ \mu M & L_e < x \le 500 \end{cases},$$

$$C_i(x,0) = \begin{cases} 1.0\ \mu M & 0 \le x \le L_i \\ 0.1\ \mu M & L_i < x \le 500 \end{cases}, \text{ and } h(x,0) = 0.78, 0 \le x \le 500,$$

where $L_c = 30$, $L_e = 30$ and $L_i = 5$. For the numerical simulations, we have considered spatial dependence of all terms containing calcium concentrations, because of the spatial heterogeneity in calcium concentrations. Unless mentioned otherwise in the text, we use the above pulse initial conditions for all simulation results reported in the remainder of this paper. To our best knowledge, this is one of the very few computational spatio-temporal models that allows the analysis of the contribution of multiple Ca^{2+} fluxes to Ca^{2+} dynamics, including entry and release, under the impact of Aβ.

The required spatio-temporal resolution brings about the computational challenges. The time step has been chosen to be very small due to the diffusion parameter, otherwise the numerical solution diverges to infinity (we have selected $dx = 0.5$ and $dt = 0.0001$). In the numerical computation, forward Euler's method is used for the time derivative, and the central difference is used for the spatial derivatives. The considered model has many terms involving different parameters. So, to find the effect corresponding to one parameter, we need to solve the model (1)–(9) many times by changing its value. In each fixed choice of the parameter values, several million time-steps are typically needed to reach the required total time, and each such time step involves thousands of spatial grid points for each parameter setting. This takes a lot of computational time if we solve the system using standard serial programming. Parallel programming is used in C-language with the help of open MPI, allowing us to save computational time. For each time-iteration, we distribute the sequential jobs involving the spatial points into free processors and compute them in a parallel way. The data have been post-processed, and all figures have been visualized and plotted in Matlab. We have used the SHARCNET supercomputer facilities (64-cores) to minimize the time to obtain results for the parallel computation.

Intracellular Ca^{2+} signals regulate many cell activities. These signals occur not only in a single cell, but also between adjacent cells in the form of calcium waves. As proof-of-concept, we have considered a one-dimensional spatial domain to capture such scenarios. In this case, the diffusion term plays a crucial role in propagating the wave initiated by a pulse of Ca^{2+} or IP_3, mentioned earlier in the initial conditions. The spatio-temporal model also follows the temporal dynamics obtainable with the model developed in [4], but accounting for spatio-temporal interactions brings about distinct advantages. Due to the given pulse on one side of the domain, the waves propagate from that side to the opposite side in the spatial domain [see Fig. 1]. These solutions are action-potential-like spikes of intracellular Ca^{2+} signals, not wave-trains. Here, the spikes appear in different time points in the spatial domain, due to the pulse type initial conditions. This

is more realistic because two different cells may produce spikes at different time points.

In Fig. 1, we plot the solutions for the intracellular Ca^{2+} concentrations for three values of Aβ levels, $a = 0, 0.2$ and 0.34. The first appearance of heterogeneous spikes over the entire spatial domain corresponding to $a = 0.2$ takes less time than in the case of $a = 0$. However, with an increment in Aβ level, e.g., $a = 0.34$, the first appearance of heterogeneous spikes takes more time than in the case of $a = 0.2$. Further increase in a causes a longer time for the spikes to appear. Moreover, all spikes fully disappear for $a > a_c$, and the solution converges to a homogeneous solution in the spatial domain, following the purely temporal dynamics of the ODE-based model [4]. It is the advanced stage of the disease, and this critical threshold a_c depends on the parameter values as well as on the initial conditions.

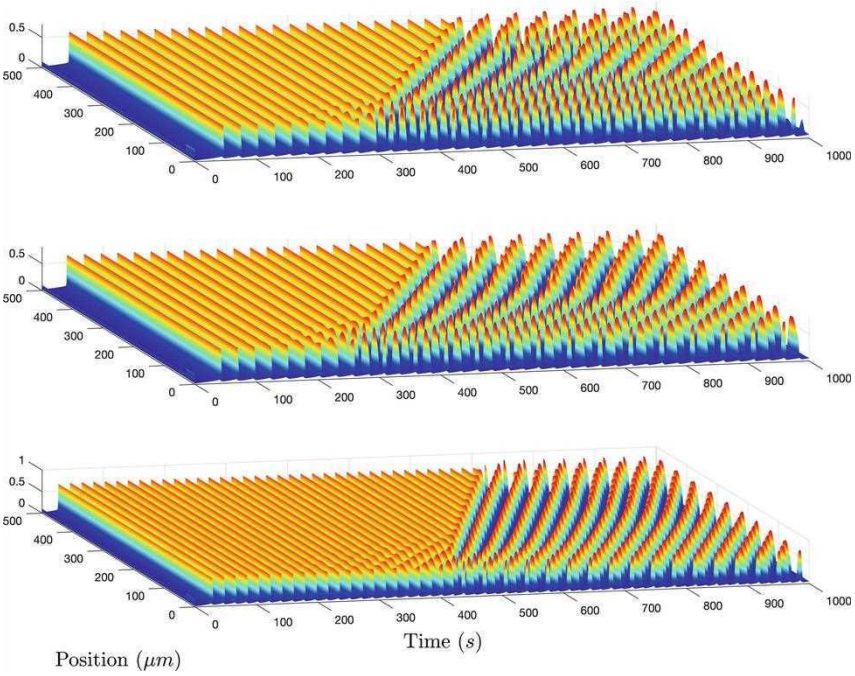

Fig. 1. Solutions corresponding to C_c for the model: $a = 0$ (top), $a = 0.2$ (middle) and $a = 0.34$ (bottom). (Color figure online)

Recall that the critical threshold of Aβ level for the model without spatial terms is $a_c = 0.6$ [4]. In this case, we can not choose the pulse type initial conditions. But, the critical threshold of Aβ level for the spatio-temporal model presented in Sect. 2, corresponding to the above initial condition, is $a_c = 0.62$. Furthermore, if we take the initial density of C_c in the pulse range $0 \leq x \leq L_c$ as $0.8\ \mu M$, then the critical threshold is shifted to $a_c = 0.63$. A wave-train solution is observed for $a < 0.63$. It seems that extra calcium concentrations injected in some parts of the cytosol cause oscillations in the system in the presence of higher Aβ levels.

These observations are also valid for a different range in the pulse structure, e.g., $L_c = 60$, $L_e = 60$ and $L_i = 5$. The shifting of the heterogeneous spikes indicates the disease building inside the cytoplasm. Therefore, the spatio-temporal extension of the earlier model helps us to predict the disease state much earlier compared to the predictions based on a purely temporal model. Note that the magnitudes of the oscillations at all spatial points are the same, but of course, they occur at different time instances as shown in Fig. 1.

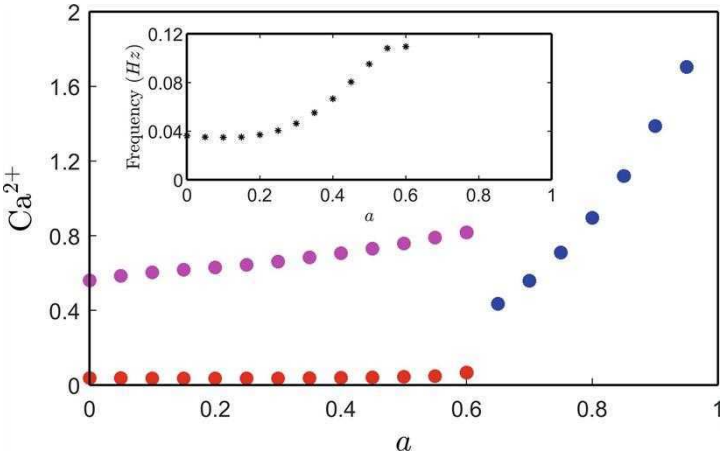

Fig. 2. Bifurcation diagram of C_c against Aβ levels: steady state (blue-dot), maximum amplitude (magenta-dot), minimum amplitude (red-dot), frequencies of the oscillations (black-star). (Color figure online)

Many processes of Ca^{2+} dyshomeostasis are difficult to explore experimentally [2,19], such as the limits of Ca^{2+} indicators and imaging methods. Aβ has been shown to cause C_c transients and C_c oscillations in astrocytes [20]. Such effects might be caused by multiple Ca^{2+} entry mechanisms as well as Ca^{2+} release from the ER [4]. These experimental results have offered us useful information in making our Aβ assumption. However, in the actual world, Aβ accumulation might take months, years, or even decades, which does not correspond to the brief timescale of Ca^{2+} fluctuations. In order to address this issue, we assumed a constant amount of Aβ in our model. We plot the amplitudes and the frequencies of intracellular Ca^{2+} for different Aβ levels in Fig. 2. In this context, we should mention that the oscillations of intracellular calcium concentration (C_c) in glial cells have a peak with an amplitude of 0.6–0.8 μM that have been reported in [17]. Here, for $a = 0$, we obtain a peak with amplitude of 0.71 μM, inside the mentioned range. On the other hand, a subset of spontaneously active thalamic astrocytes exhibits C_c oscillations with an average frequency of 0.019 Hz has been found in [18]. The model considered in this paper produces 0.036 Hz, a spatial average of frequencies in the whole domain without Aβ (i.e., $a = 0$). A similar type of frequency increase is observed in the astrocytic Ca^{2+} experimentally after the Aβ injection [21]. Therefore, the

spatio-temporal model is consistent with the experimental data reported earlier in the literature.

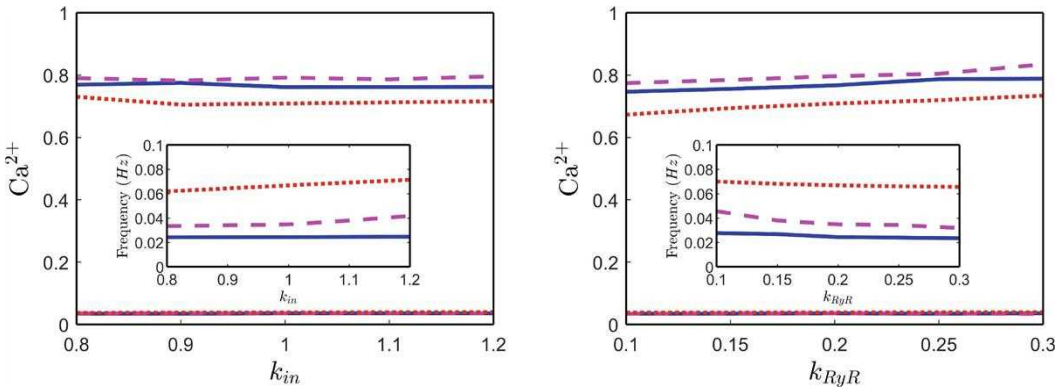

Fig. 3. Effect of bifurcation parameters on C_c and its frequencies for different Aβ levels with other fixed parameters given in Table 2: $a = 0.2$ (solid-blue), $a = 0.3$ (dashed-magenta) and $a = 0.4$ (dotted-red). (Color figure online)

Now, we turn our attention to the effect of the parameters k_{in} and k_{RyR} [see formulas in (10)] on the resulting intracellular Ca^{2+} signals and the frequencies. For each of the bifurcation parameters, the range of the oscillations of the intracellular calcium concentrations and corresponding frequencies is plotted in Fig. 3. In the plot, solid (blue), dashed (magenta) and dotted (red) curves are corresponding to $a = 0.2, 0.3$ and 0.4, respectively. For the case of the parameter k_{in}, the amplitudes of the oscillations are not changing significantly in the considered range $k_{in} \in [0.8, 1.2]$, but the frequency increases with k_{in}. On the other hand, with an increase in the bifurcation parameter $k_{RyR} \in [0.1, 0.3]$, the amplitudes of the oscillations increase, and the frequencies decrease. These results are similar to the results that were obtained based on the purely temporal model, but now the spikes are heterogeneously distributed over the spatial domain.

For a fixed Aβ level, the first appearance of the heterogeneous spikes corresponding to a lower value of k_{in} takes less time compared to a higher value of k_{in}. The opposite case happens when we analyze the bifurcation parameter k_{RyR}. These bifurcation parameters k_{in} and k_{RyR} are correlated with the Aβ levels.

Based on experimental results reported earlier in [16], it was suggested that the calcium increases its frequency at the lower affinity of SERCA1 enzyme. In our spatio-temporal model, the parameter ν_3 is the maximum SERCA pump flux, and we choose ν_3 as a controlling parameter. According to the model (1)–(9), an increase in the removal rate parameter (ν_3) in the cytosol decreases Ca^{2+} concentration in the cytosol but increases Ca^{2+} in the endoplasmic reticulum. We have carried out the simulation and plotted the magnitudes and the frequencies of the oscillations of intracellular calcium densities for the bifurcation parameter ν_3 in Fig. 4. The amplitude of the oscillations of Ca^{2+} in cytosol increases with ν_3.

However, the parameter ν_3 is anti-correlated with the frequency. An increase in ν_3 causes a slow rise of Ca^{2+} in the cytosol to a threshold where the endoplasmic reticulum takes over the autocatalytic release of Ca^{2+} and hence it decreases the frequency of the oscillations.

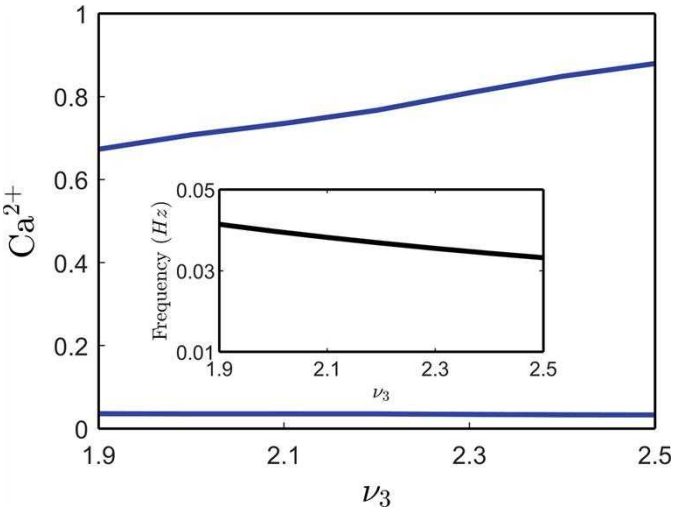

Fig. 4. Bifurcation diagram of C_c and the corresponding frequency against the parameter ν_3 with a fixed Aβ level ($a = 0.2$). (Color figure online)

Due to the differences in extracellular K^+ concentrations from cell to cell, the resulting resting membrane potential may also vary [22]. This resting membrane potential affects the open probability of VGCC, and hence it affects J_{VGCC} and the intracellular calcium dynamics [23]. Figure 5 represents the frequencies of C_c oscillations depending on the extracellular K^+ concentrations for different Aβ levels. With an increase in the resting membrane potentials, the frequency of intracellular Ca^{2+} oscillations increases, and further gain converges to the steady-state solutions. Recall that our studies have demonstrated that the frequency increases with Aβ levels [see Fig. 2], and the same happens for different resting membrane potentials. Therefore, a higher resting membrane potential indicates a further progression of the disease state. Overall, the developed model and our results suggest that we should expect a smaller contribution to the dysregulation of cytosolic Ca^{2+} levels from VGCCs compared to Aβ. This happens because of the robustness of cytosolic Ca^{2+}under Aβ [8].

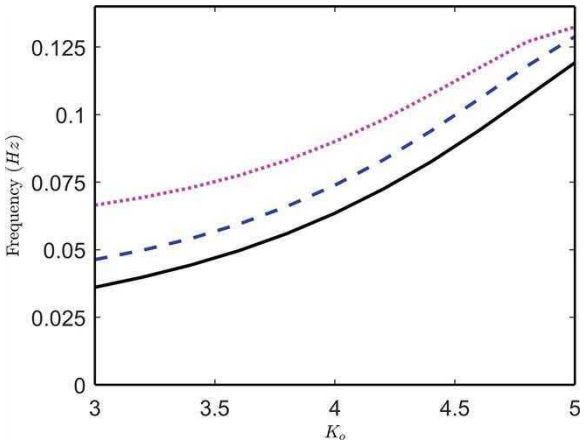

Fig. 5. Bifurcation diagram of the frequencies of C_c against the parameter K_o for different Aβ levels: $a = 0$ (solid-black), $a = 0.3$ (dashed-blue) and $a = 0.4$ (dotted-magenta). (Color figure online)

4 Conclusions

Many chemicals are available in the brain cell, and calcium is the most tractable, used for experimental validations. The calcium concentration oscillates in the living brain cell, but remains steady in the dead cell. Alzheimer's disease (AD) causes neuronal death in the brain, and hence the calcium dynamics of a cell reflects the disease state. In this work, we have studied the AD progression in a heterogeneous environment in the cytoplasm with the help of calcium dynamics. The amyloid-beta peptide plays an essential role in the oscillating dynamics of intracellular and extracellular calcium concentrations. A pulse type of initial conditions has been chosen for the simulations in order to better reflect heterogeneity in the cytoplasm.

The amplitude of intracellular calcium oscillations increases with the amyloid-beta levels. The same happens for the frequencies. But, after a critical threshold of amyloid-beta level, the calcium concentration stops its oscillations and remains in a homogeneous steady-state over the domain. This critical threshold depends on additional calcium concentrations injected in the cytosol but not much on the range of injected domain, dictated by the pulse type initial conditions. We have studied the dynamics of biochemical processes with models by varying different parameters. The parameter ν_3 involved in the SERCA pump flux has a pronounced effect on the frequency of intracellular calcium concentrations. Also, an increase in the resting membrane potential increases the frequency for a fixed amyloid-beta level. The additional influx negatively impacts the astrocytic homeostasis irrespective of the other parameters. We note that several computational models are available in the literature based on Ca^{2+} mechanisms [2–4]. They are presented in a single framework and contain VGCCs and RyRs in astrocytes, but all of them are ODE models. The novelty of our work is that it goes beyond this conventional approach. This work has also important practical significance since our parametric study can provide a guidance to

the development of different therapies targeting different Aβ levels, signals, or channels.

In general, it is quite challenging to establish a complete model of Aβ-mediated multi-pathway calcium dynamics in the disease progression, and simulation-based mathematical models help study the dynamics with different parameters. We have accounted for some of the key parameters to capture different pathways, while others have been left out for further studies. As a result, different pathways simultaneously suggest being more effective in targeting combination therapies to provide new insight into the treatment of AD. Furthermore, along with the amyloid-beta, the tau protein also plays an essential role in AD progression [24,25]. Therefore, following those recent works and introducing the tau dynamics into the calcium model would be a natural generalization of the model presented here. Finally, an extension of the presented spatio-temporal model to account for more realistic brain topologies would lead to further insights into the disease progression.

Acknowledgements. Authors are grateful to the NSERC and the CRC Program for their support. RM is also acknowledging support of the BERC 2022–2025 program and Spanish Ministry of Science, Innovation and Universities through the Agencia Estatal de Investigacion (AEI) BCAM Severo Ochoa excellence accreditation SEV-2017–0718 and the Basque Government fund AI in BCAM EXP. 2019/00432. This research was enabled in part by support provided by SHARCNET (www.sharcnet.ca) and Digital Research Alliance of Canada (www.alliancecan.ca).

References

1. Schäfer, A., et al.: Predicting brain atrophy from tau pathology: a summary of clinical findings and their translation into personalized models. J Brain Multiphys. **2**, 100039 (2021)
2. Latulippe, J., Lotito, D., Murby, D.: A mathematical model for the effects of amyloid beta on intracellular calcium. PLoS ONE **13**, e0202503 (2018)
3. Shaheen, H., Singh, S., Melnik, R.: A neuron-glial model of exosomal release in the onset and progression of Alzheimer's disease. Front. Comput. Neurosci. **15**, 79 (2021)
4. Liu, L., Gao, H., Zaikin, A., Chen, S.: Unraveling Aβ-mediated multi-pathway calcium dynamics in astrocytes: implications for Alzheimer's Disease treatment from simulations. Front. Physiol. **12**, 767892 (2021)
5. Verkhratsky, A., et al.: Astroglial atrophy in Alzheimer's disease. Pflügers Archiv-Eur. J. Physiol. **471**(10), 1247–1261 (2019)
6. De Pittà, M., et al.: Glutamate regulation of calcium and IP3 oscillating and pulsating dynamics in astrocytes. J. Biol. Phys. **35**(4), 383–411 (2009)
7. Demuro, A., Parker, I., Stutzmann, G.E.: Calcium signaling and amyloid toxicity in Alzheimer disease. J. Biol. Chem. **285**(17), 12463–12468 (2010)
8. Lim, D., et al.: Amyloid beta deregulates astroglial mGluR5-mediated calcium signaling via calcineurin and Nf-kB. Glia **61**, 1134–1145 (2013)
9. Jafri, M.S., Keizer, J.: On the Roles of Ca^{2+} Diffusion, Ca^{2+} Buffers, and the Endoplasmic Reticulum in IP_3-lnduced Ca^{2+} Waves. Biophys. J . **69**, 2139–2153 (1995)

10. Semyanov, A., Henneberger, C., Agarwal, A.: Making sense of astrocytic calcium signals-from acquisition to interpretation. Nat. Rev. Neurosci. **21**, 551–564 (2020)
11. Agulhon, C., et al.: What is the role of astrocyte calcium in neurophysiology? Neuron **59**(6), 932–946 (2008)
12. Ullah, G., Jung, P., Cornell-Bell, A.H.: Anti-phase calcium oscillations in astrocytes via inositol (1, 4, 5)-trisphosphate regeneration. Cell Calcium **39**(3), 197–208 (2006)
13. Alberdi, E., et al.: Ca^{2+}-dependent endoplasmic reticulum stress correlates with astrogliosis in oligomeric amyloid β-treated astrocytes and in a model of Alzheimer's disease. Aging Cell **12**, 292–302 (2013)
14. Alves, V.S., et al.: Calcium signaling in neurons and glial cells: role of Cav1 channels. Neuroscience **421**, 95–111 (2019)
15. Atri, A., et al.: A single-pool model for intracellular calcium oscillations and waves in the Xenopus Laevis oocyte. Biophys. J . **65**, 1727–1739 (1993)
16. Camacho, P., Lechleiter, J.D.: Increased frequency of calcium waves in Xenopus Laevis oocytes that express a calcium-ATPase. Science **260**, 226–229 (1993)
17. Charles, A.C., Merrill, J.E., Dirksen, E.R., Sanderson, M.J.: Intercellular signalling in glial cells: calcium waves and oscillations in response to mechanical stimulation and glutamate. Neuron **6**, 983–992 (1991)
18. Parri, H.R., Crunelli, V.: Pacemaker calcium oscillations in thalamic astrocytes in situ. NeuroReport **12**, 3897–3900 (2001)
19. Vassilis, C., Moustafa, A.A.: Neurocomputational models of Alzheimer's disease. Scholarpedia (2017)
20. Alberdi, E., Wyssenbach, A., Alberdi, M., Sánchez-Gómez, M.V., Cavaliere, F., Rodríguez, J.J., Verkhratsky, A., Matute, C.: Ca^{2+}-dependent endoplasmic reticulum stress correlates with astrogliosis in oligomeric amyloid β-treated astrocytes and in a model of Alzheimer's disease. Aging Cell **12**(2), 292–302 (2013)
21. Takano, T., et al.: Two-photon imaging of astrocytic Ca2+ signaling and the microvasculature in experimental mice models of Alzheimer's disease. Ann. N. Y. Acad. Sci. **1097**, 40–50 (2007)
22. Anderson, S., Brismar, T., Hansson, E.: Effect of external K^+, Ca^{2+}, and Ba^{2+} on membrane potential and ionic conductance in rat astrocytes. Cell. Mol. Neurobiol. **15**, 439–450 (1995)
23. Bellot-Saez, A., Kekesi, O., Morley, J.W., Buskila, Y.: Astrocytic modulation of neuronal excitability through K^+ spatial buffering. Neurosci. Biobehav. Rev. **77**, 87–97 (2017)
24. Pal, S., Melnik, R.: Pathology dynamics in healthy-toxic protein interaction and the multiscale analysis of neurodegenerative diseases. In: Paszynski, M., Kranzlmüller, D., Krzhizhanovskaya, V.V., Dongarra, J.J., Sloot, P.M.A. (eds.) ICCS 2021. LNCS, vol. 12746, pp. 528–540. Springer, Cham (2021). https://doi.org/10.1007/978-3-030-77977-1_42
25. Pal, S., Melnik, R.: Nonlocal models in the analysis of brain neurodegenerative protein dynamics with application to Alzheimer's disease. Sci. Rep. **12**, 7328 (2022)